Dynamics of the Intraseasonal Oscillations in the Indian Ocean South Equatorial Current

LEI ZHOU AND RAGHU MURTUGUDDE

Earth System Science Interdisciplinary Center, University of Maryland, College Park, College Park, Maryland

MARKUS JOCHUM

National Center for Atmospheric Research, Boulder, Colorado*

(Manuscript received 21 November 2006, in final form 20 April 2007)

ABSTRACT

The spatial and temporal features of intraseasonal oscillations in the southwestern Indian Ocean are studied by analyzing model simulations for the Indo-Pacific region. The intraseasonal oscillations have periods of 40–80 days with a wavelength of ~650 km. They originate from the southeastern Indian Ocean and propagate westward as Rossby waves with a phase speed of ~25 cm s^{-1} in boreal winter and spring. The baroclinic instability is the main driver for these intraseasonal oscillations. The first baroclinic mode dominates during most of the year, but during boreal winter and spring the second mode contributes significantly and often equally. Consequently, the intraseasonal oscillations are relatively strong in boreal winter and spring. Whether the atmospheric intraseasonal oscillations are also important for forcing the oceanic intraseasonal oscillations in the southwestern Indian Ocean needs further investigation.

1. Introduction

Oceanic intraseasonal oscillations (OISOs) are found to be an important part of the ocean dynamics in the upper layer over the global oceans (e.g., Kessler et al. 1995; Farrar and Weller 2006; Jochum and Malanotte-Rizzoli 2003). In the tropical Indian Ocean, the OISOs are enhanced due to the internal oceanic instability and the response to the intraseasonal atmospheric forcing (Waliser et al. 2003; Reppin et al. 1999; Sengupta et al. 2001). As for the southern Indian Ocean, there have been some observational and modeling studies in the southeastern Indian Ocean (SEIO). Feng and Wijffels (2002) analyzed the satellite altimeter data and reported that the wavelength of the OISOs in SEIO is from 600 to 900 km (the length scale is from 100 to 150 km), the period is from 40 to 80 days, and the westward phase speed is from 15 to 19 cm s^{-1}. They attribute the enhanced OISOs during the second half of the year to the baroclinic instability, which drew most energy from the available potential energy associated with the Indonesian Throughflow (ITF). Yu and Potemra (2006) concluded that the barotropic and the baroclinic instabilities contribute almost equally to the genesis in the Indo-Australian basin, by analyzing a numerical ocean model. They found that the baroclinic instability was sensitive to the warmer and fresher ITF and the barotropic instability is attributable to the strong zonal shear between the Eastern Gyral Current and the South Equatorial Current, which is strengthened by the ITF. In addition to the close relations with the ITF (Potemra et al. 2002), the OISOs in SEIO also respond to the intraseasonal atmospheric forcing (Sprintall et al. 2000; Han 2005; Iskandar et al. 2005, 2006). The OISOs in SEIO propagate westward as Rossby waves, which may influence the southwestern Indian Ocean (SWIO). For example, Sengupta et al. (2001) used a model driven by the National Centers for Environmental Prediction (NCEP) data to show that the 30–50-day oscillations appeared as a result of the westward-propagating Rossby waves and were enhanced by the oceanic instability in the western equatorial Indian Ocean.

To the best of our knowledge, there have been neither systematic observations nor modeling studies of

* The National Center for Atmospheric Research is sponsored by the National Science Foundation.

Corresponding author address: Lei Zhou, Computer and Space Sciences Bldg. 2330, University of Maryland, College Park, College Park, MD 20742.
E-mail: lzhou@atmos.umd.edu

DOI: 10.1175/2007JPO3730.1

OISOs thus far in SWIO (e.g., Murtugudde and Busalacchi 1999). Therefore, the purpose of this paper is to describe the spatial and temporal dynamic properties of OISOs in SWIO, and then to provide the dynamic reasons for their development. In section 2, the model is described and the model results are compared with the observations. In section 3, the features of OISOs in SWIO are described. In section 4 the dynamic reasons for their genesis and enhancement are explored by analyzing the stability and the vertical modes of the ocean currents. The conclusions and discussions are presented in section 5.

2. Model description and comparison

a. Model description

The model used in this study is a reduced-gravity, sigma-coordinate, primitive equation OGCM, with a horizontal resolution of ⅓° in latitude and ½° in longitude over the Indo-Pacific domain covering 30°S–30°N, 32°E–76°W (Murtugudde et al. 1996, 1998). There are 15 sigma layers in the vertical below the variable-depth mixed layer with a resolution of ~20 m in the thermocline in the SWIO, so that the vertical oscillation in the interior ocean can be adequately resolved. The surface mixed layer is determined by the hybrid mixing scheme of Chen et al. (1994), which explicitly accounts for the entrainment induced by the surface turbulent kinetic energy, shear-induced dynamic stability mixing, and convective mixing to remove static instabilities. The last sigma layer is a prognostic variable whereas the other sigma layers are specified constant fractions of the total depth below the mixed layer to the motionless abyssal layer. The model is driven by the climatological weekly NCEP reanalysis winds (see Murtugudde et al. 2000 for details). The model outputs for all the analyses presented here are weekly mean fields from the last 20 yr of a 270-yr simulation. Note that we only focus on OISOs in the climatological run to avoid contributions from interannual forcings (also see Jochum and Murtugudde 2005).

b. Model–data intercomparisons

The OGCM has been reported in many previous applications demonstrating its ability to simulate the ocean dynamics and thermodynamics reasonably well in the tropical oceans. The westward South Equatorial Current (SEC) stretches from 8° to 20°S, which is consistent with the observations in Schott et al. (2002).

Obviously, what we are concerned most with is the model's ability to resolve OISOs in the Indian Ocean. Since we intend to study the internal intraseasonal variability in the ocean, the model is driven by the climatological winds as in Jochum and Murtugudde (2005). This also means that we do not expect perfect matches between the model results and interannual observations. The root-mean-square (RMS) of the intraseasonal sea surface height anaomalies (SSHAs), which are high-pass filtered with a cutoff frequency of 100 days, and the uncertainty of its annual mean values from the model simulation and the satellite observations are shown in Fig. 1. The eddy kinetic energy (EKE) as determined from SSHA is well captured in the model, especially the two zonal bands of high EKE at 5° and 10°S. Moreover, the high EKE along the Somali coast and in the southern Bay of Bengal are also resolved. The main shortcomings of the model are the weak EKE along the Sumatra coast and along 10°S west of 80°E.

In our model, the main period of the OISOs in SEIO is from 40 to 80 days. The wavelength is about 700 km to the east of 110°E and extends to about 1000 km to the west of this longitude. These estimations are almost identical to the observations reported in Feng and Wijffels (2002), which examined the intraseasonal variability in SEIO by analyzing the Ocean Topography Experiment (TOPEX)/Poseidon altimeter data and World Ocean Circulation Experiment (WOCE) data. Therefore, with these comparisons between the model data and observations in SEIO, we conclude that the model ably resolves both the spatial and temporal properties of OISOs in the Indian Ocean.

3. Properties of OISOs in the SWIO

All calculations that follow are based on the weekly mean model outputs. Before describing the properties of OISOs in SWIO, we would like to confirm that they are a significant part of the variability in the SWIO. The standard deviations (STDs) of the intraseasonal SSHAs account for 20%–40% of the total STDs of SSHAs in the zonal belt. The maximum ratio can be as large as 50%. Therefore, OISOs are indeed a nonnegligible component of the variability in the region and are important for understanding the oceanic processes in the SWIO.

Figure 2 shows the wavelet spectrum of SSHAs at 6°S, 66°E. This point is chosen because the STDs of the intraseasonal SSHAs at this point are large. The obvious peak is from 40 to 90 days, centered at 80 days. The OISOs in SWIO strengthen in boreal winter and spring. Their wavelength is ~650 km, which is comparable to the wavelength of 600–900 km in SEIO (Feng and Wijffels 2002). There is a westward propagation with a phase speed of about 25 cm s^{-1} in boreal winter and spring (Fig. 3). For example, there is a strong positive signal starting at 77°E in early November and ending at

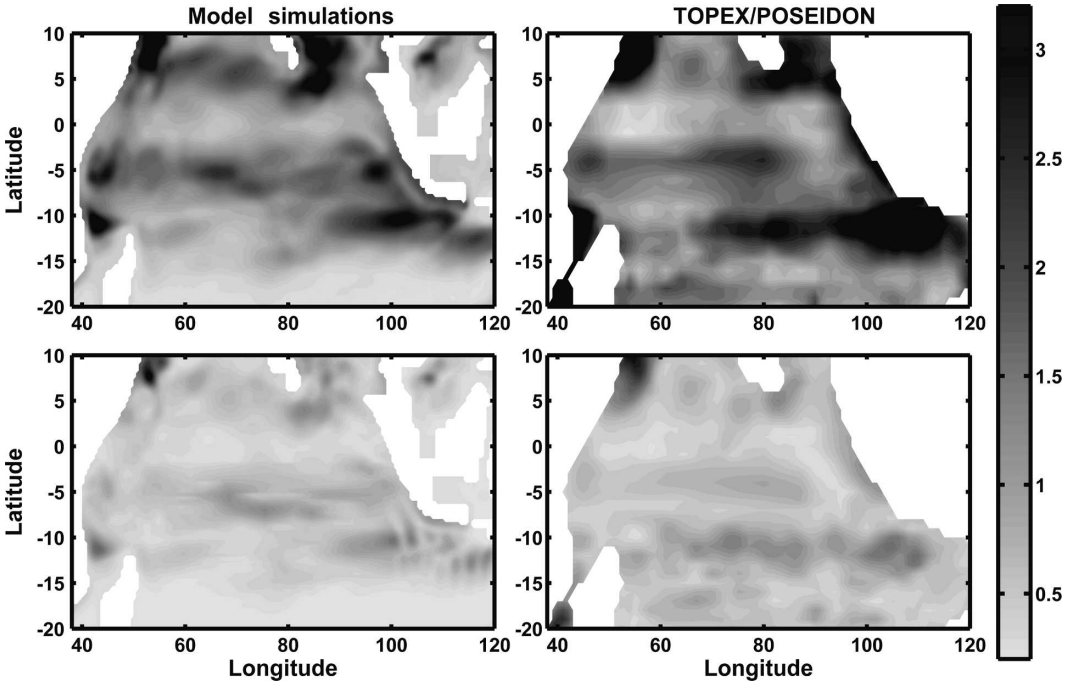

FIG. 1. (top) RMS (cm) of intraseasonal SSHAs of 20-yr model simulations and TOPEX/Poseidon data from 1992 to 2006 and (bottom) its uncertainty (cm) defined as the RMS of its annual mean values for the model and the TOPEX/Poseidon data.

65°E in late December of the first year. The phase speed reduces to about 17 cm s^{-1} in other seasons, as seen by a positive anomaly at 80°E in late March of the second year reaching 60°E in late August. The seasonal change of phase speed is attributable to the variability of ocean stratification. We also note that the phase speed changes with longitude. For instance, there is a negative signal around 75°E in February of the second

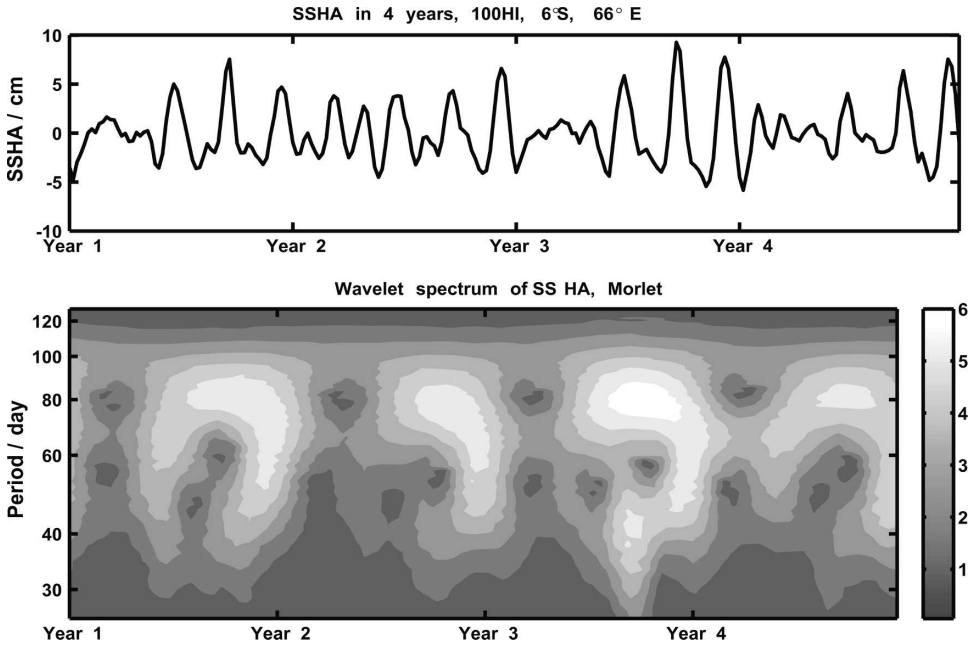

FIG. 2. Intraseasonal SSHAs (cm) at 6°S, 66°E for four years and the corresponding wavelet spectrum (cm).

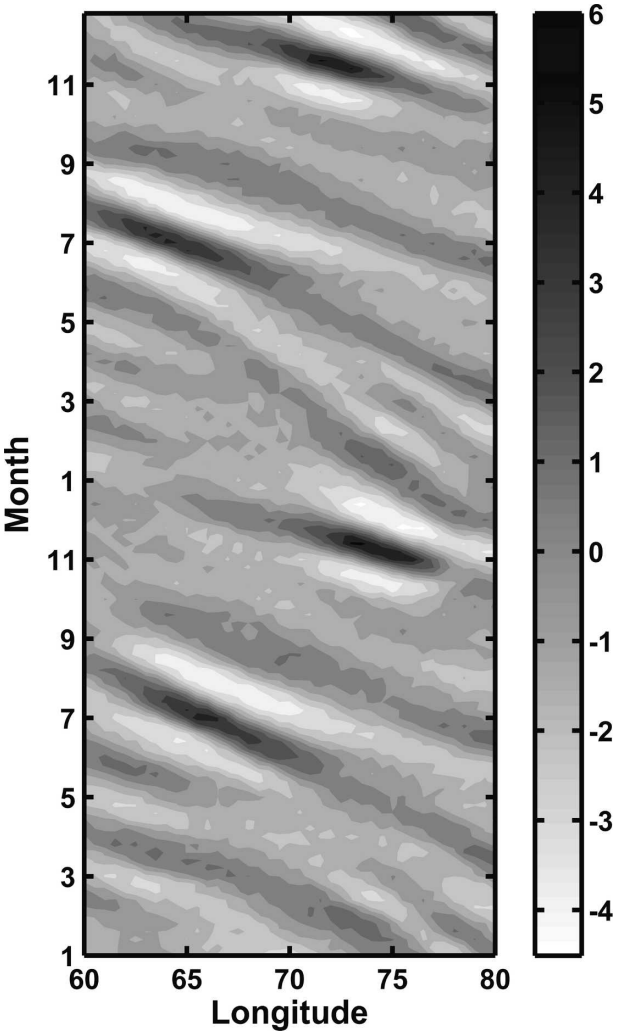

FIG. 3. Longitude–time plot of intraseasonal SSHAs along 8°S (cm).

year, which speeds up at about 67°E in May. This phase speed change is caused by the interactions between the local forcing and the Rossby waves (Wang et al. 2001). The range of estimated phase speed is comparable to the theoretically expected range. In addition, the dispersion relation of the westward-propagation signals is consistent with that of the linear theoretical Rossby waves (not shown). Therefore, it can be concluded that the westward propagations of the signals are caused by the Rossby waves (Masumoto and Meyers 1998).

4. Dynamic processes responsible for OISOs in the SWIO

Generally, there are two reasons for the genesis of OISOs. One is external forcing (e.g., intraseasonal winds) and the other is internal instability (e.g., local barotropic and baroclinic instabilities). Both are explored in this section to determine the dynamic reasons for OISOs in the SWIO.

High-frequency wind stresses are one of the leading candidates. However, the climatological wind stresses used to force the model do not have pronounced peaks in the intraseasonal band. The low-frequency currents are significantly correlated with the geostrophic flow, which indicates that they are generally driven by the winds and satisfy the Sverdrup relation. On the other hand, the correlations between the intraseasonal currents (i.e., OISOs) and the geostrophic flow are statistically negligible over the entire southern Indian Ocean, which indicates that the OISOs in SWIO in our model simulation are not caused by the local response to external wind forcing.

Naturally, we assume that OISOs in SWIO are attributable to the internal instabilities of the ocean currents. The prerequisite for the instability analysis is the determination of the basic flow (Pedlosky 1987), where by definition, the basic flow is the flow that is not disturbed by the eddy flow. Thus, it is not simply equivalent to the mean flow. In the model, the low-pass-filtered velocity has a large STD for the entire 20-yr period but small STDs in each month. On the contrary, the high-pass-filtered velocity has large STDs in each month but a relatively small STD for the 20-yr period. Since the model is driven by the climatological winds, the STD of the wind stresses is large while the wind stress in each month is identically the same (the STD of interannual variability is zero). The low-frequency velocity is mainly a response to external wind forcing, hence it has a large annual cycle but changes very little in the same month of different years [interannual variability is small; see Jochum and Murtugudde (2005)]. However, the high-frequency velocity is mainly caused by the internal oceanic processes, especially eddies, hence changes significantly in the same month of different years, even though the wind forcing is the same. With these considerations, various cutoff periods are tried. It turns out that the low-pass-filtered velocity with a cutoff period of 150 days is the optimal basic flow for the model outputs.

a. Barotropic and baroclinic instabilities in the SWIO

The necessary condition for barotropic instability is that $dq/dy = \beta - (\partial^2 U/\partial y^2)$, where q is the quasigeostrophic potential vorticity (QGPV) and U is the basic flow, should change sign in the domain under consideration. Figure 4a shows the annual mean dq/dy in the SWIO, which is always positive in SEC, because the relative vorticity gradient $\partial^2 U/\partial y^2$ is too small to overcome the planetary vorticity gradient β. Since the con-

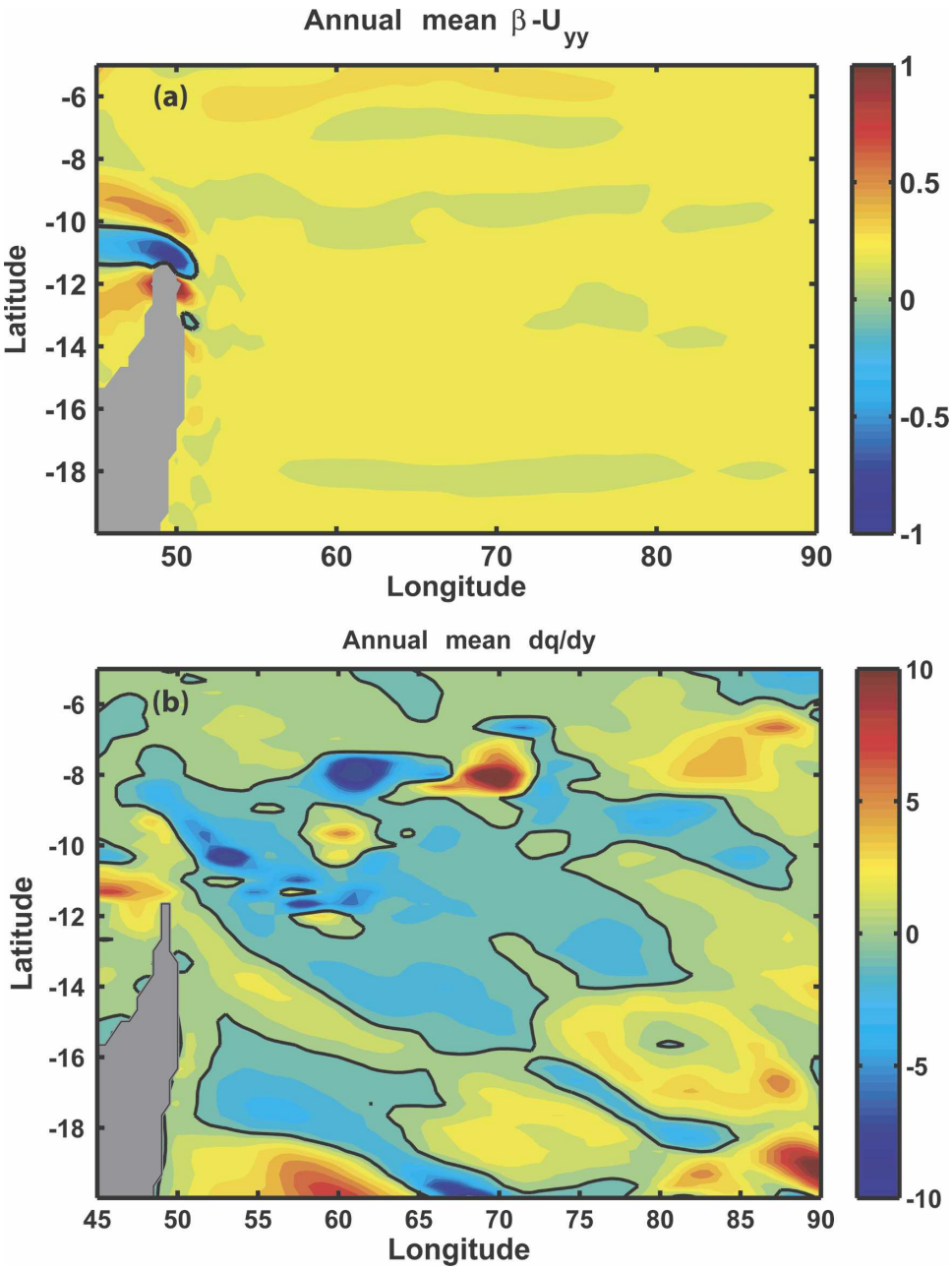

FIG. 4. Annual mean (10^{10} m^{-1} s^{-1}) of (a) $dq/dy = \beta - (\partial^2 U/\partial y^2)$ and (b) $dq/dy = \beta - \partial^2 U/\partial y^2 - \partial/\partial z[(f_0^2/N^2)(\partial U/\partial z)]$. The black contour is the contour of zero.

dition that dq/dy change sign is a necessary condition for barotropic instability, it is very unlikely that the barotropic instability can be triggered in SWIO.

The necessary condition for baroclinic instability is also that the meridional gradient of QGPV (viz., dq/dy) should change sign in the domain. However, in the baroclinic situation,

$$dq/dy = \beta - (\partial^2 U/\partial y^2) - (\partial/\partial z)[(f_0^2/N^2)(\partial U/\partial z)].$$

Figure 4b shows the distribution of the annual mean dq/dy in the SWIO. Since the areas with positive and negative signs are similar and the positive and negative magnitudes are comparable, the baroclinic instability is very likely to occur in the SWIO. However, since satisfying the necessary condition alone cannot guarantee the triggering of an instability, the energy conversions are examined with the model fields below.

The energy conversions caused by the barotropic and

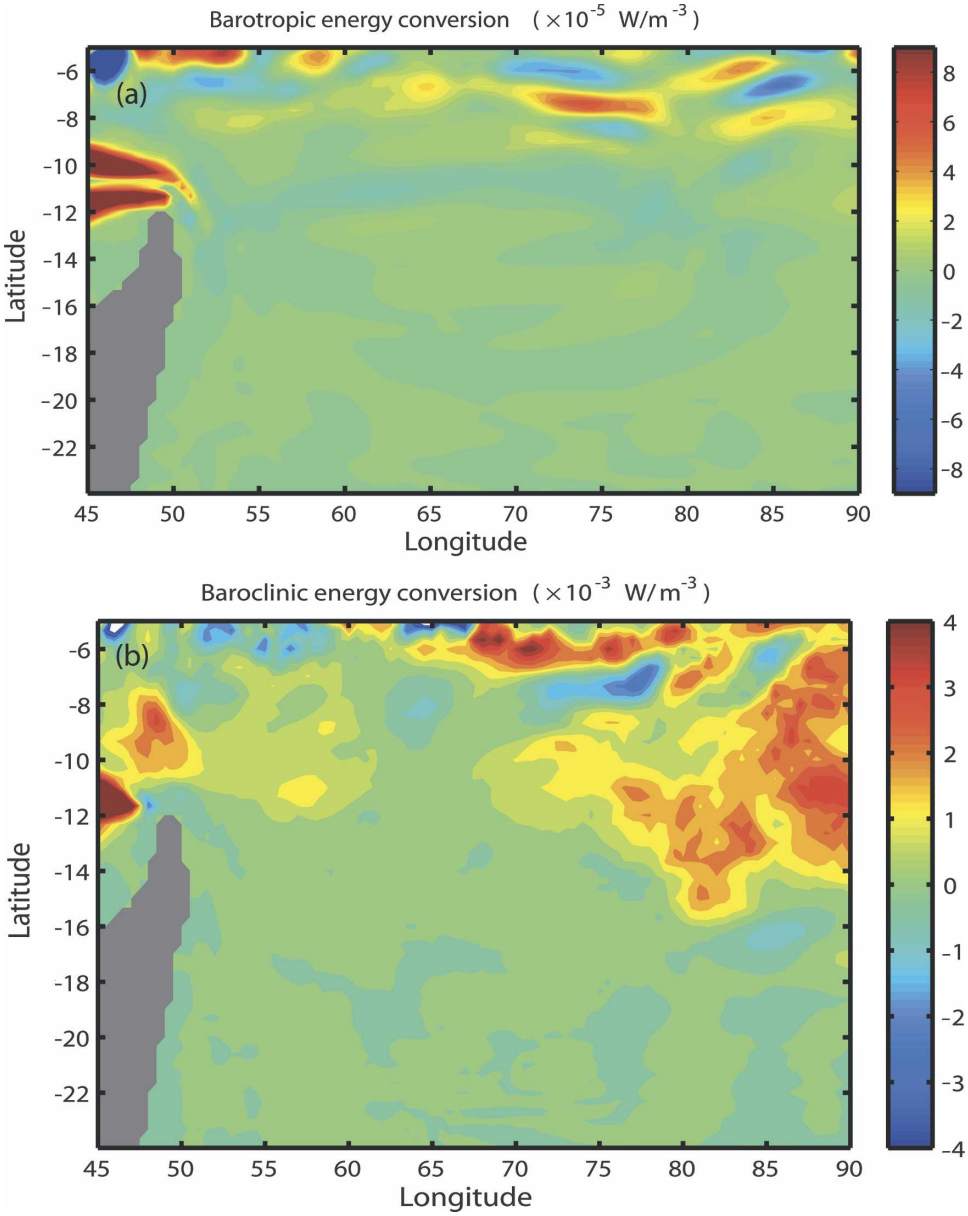

FIG. 5. (a) Barotropic and (b) baroclinic energy conversions averaged over 20 yr and above the thermocline in the SWIO.

the baroclinic instability are calculated with the equation in Weisberg and Weingartner (1988). The barotropic energy conversion is small in the southern Indian Ocean, as shown in Fig. 5a. South of 10°S, the barotropic energy conversion is almost zero. Between 5° and 10°S, the barotropic energy conversion is slightly larger because the horizontal shears are large. However, the barotropic energy conversion is always smaller than 10^{-4} W m^{-3} because the zonal shears are not very strong. The baroclinic energy conversion is at least two orders of magnitude larger than the barotropic energy conversion (Fig. 5b) and can be as large as 4×10^{-3} W m^{-3}. Thus, the energy conversion between eddy flow and mean flow in the southern Indian Ocean should be dominated by the baroclinic energy conversion. This is consistent with the above calculations of the necessary conditions for the instability that the barotropic instability is not likely to contribute, while the baroclinic instability dominates in the SWIO.

b. *Seasonality of baroclinic energy conversion and OISOs*

Monthly mean baroclinic energy conversion for four months representing the four seasons are shown in Fig.

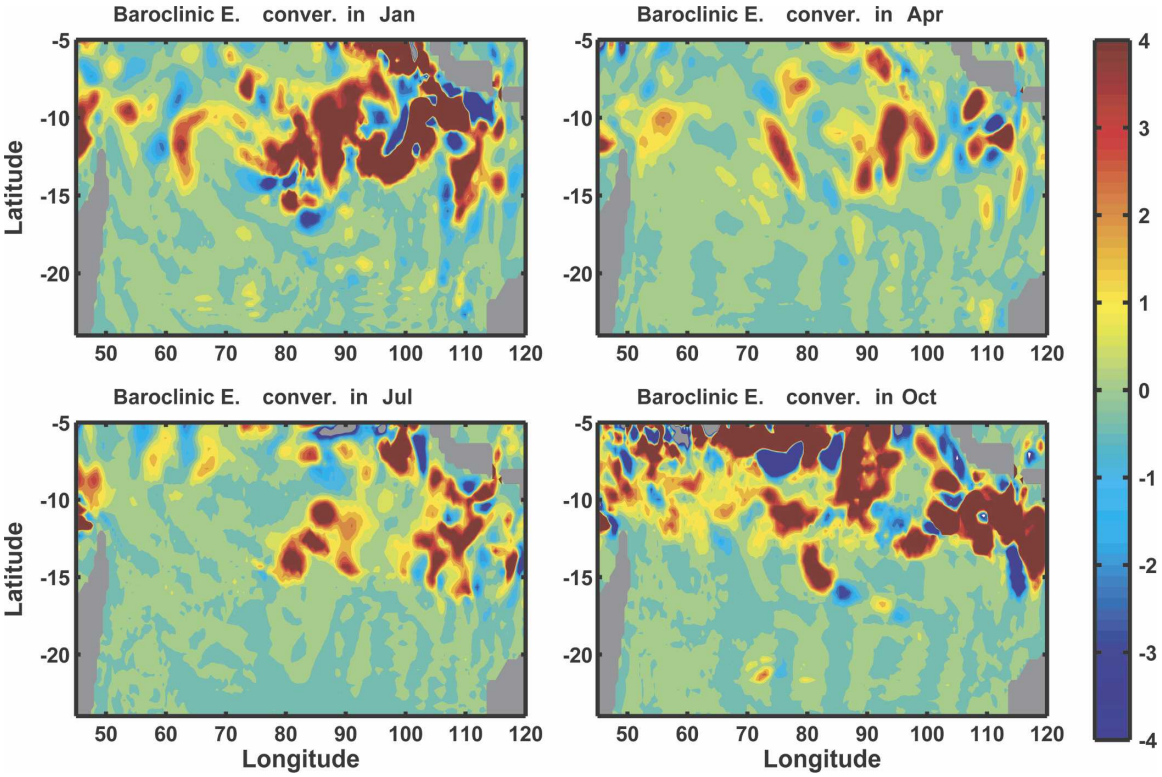

FIG. 6. Baroclinic energy conversion (10^{-3} W m^{-3}) averaged over 20 yr and above the thermocline in four months.

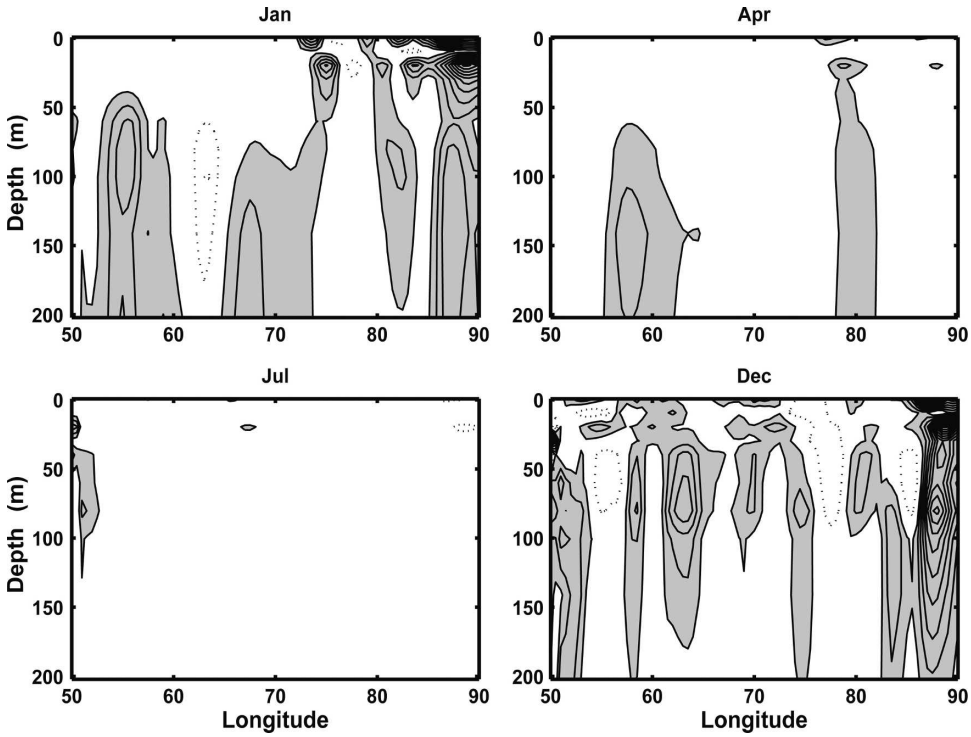

FIG. 7. Longitude–depth plots of baroclinic energy conversions for January, April, July, and December. The contour interval is 1×10^{-3} W m^{-3}. Regions with positive values are shaded.

6. In SWIO, the seasonal changes are pronounced. In April and July, the baroclinic energy conversion is small with only a few patches of moderate conversion rate of 10^{-3} W m^{-3}. At the end of boreal summer, the conversion rates begin to increase and in October, they are larger than 2×10^{-3} W m^{-3} in almost the entire SWIO exceeding 10×10^{-3} W m^{-3} in some areas. During boreal winter, the baroclinic conversion rates decrease, but there are still large areas with conversion rates of 2×10^{-3} W m^{-3}. The seasonal changes in Fig. 6 are consistent with the seasonal changes of intraseasonal zonal currents, which confirm that the strong OISOs in the SWIO are caused by baroclinic instability.

Figure 7 shows the longitude–depth section of baroclinic energy conversion, averaged between 8° and 10°S for the four months. The conversions in SWIO are strong in January and October but negligible in April and July, which is consistent with the seasonal variability shown in the horizontal plain (Fig. 6). However, the strong conversions in the SWIO are not at the surface, but in the depth range from 50 to 100 m, which coincides with the upper part of the thermocline. This thermocline intensification is examined further in section 4c.

Generally, baroclinic instability is mainly caused by the vertical velocity shear. Figure 8 shows the vertical velocity shears around the thermocline (~100 m) where they reach maximum, along with the corresponding baroclinic energy conversions. In boreal winter and spring, the vertical velocity shear increases due to the thermocline-intensified zonal advection from the SEIO (see section 4c). Thus, the strong baroclinic energy conversion is caused by a larger density gradient around the thermocline and by the vertical shear between the SEC and the eastward currents underneath. Moreover, the patterns in Fig. 8 also show a similar westward propagation as in Fig. 3, especially the vertical velocity shear from 80° to 70°E. This indicates that the large vertical shears around the thermocline are caused by the strong currents propagating from the SEIO.

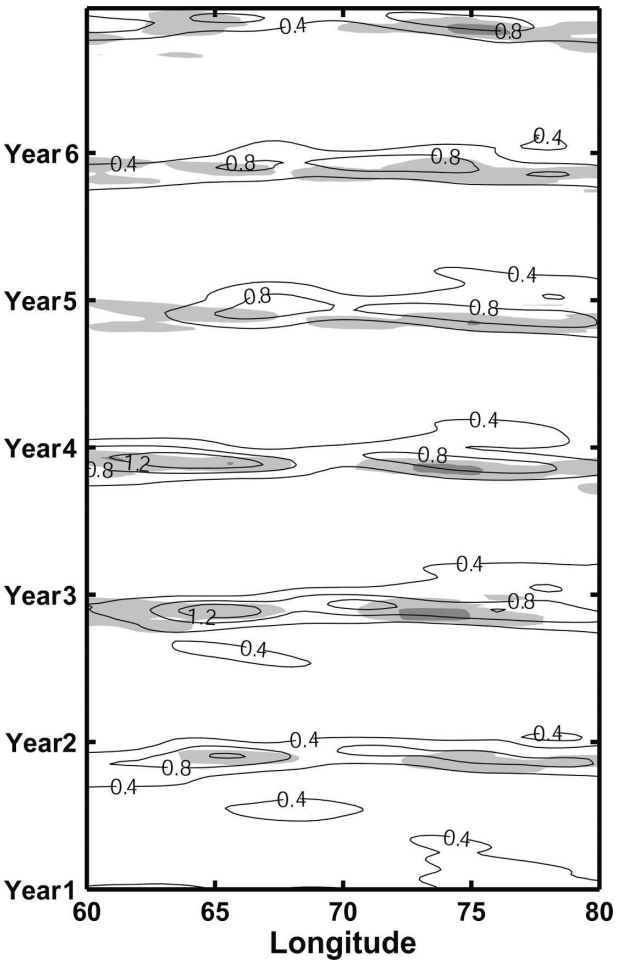

FIG. 8. Vertical shears (10^{-3} s^{-1}) of zonal currents around the thermocline (~100 m) along 8°S for six random years (contours) superposed with the baroclinic energy conversions (shaded area). The light gray area shows the energy conversion of 1×10^{-2} W m^{-3}, and the dark gray shows that of 4×10^{-2} W m^{-3}.

c. Dominant baroclinic modes

To explain why the baroclinic energy conversions or the vertical shears of horizontal currents are intensified around the thermocline (Fig. 7), a modal decomposition method is applied. The horizontal velocities u and v are decomposed into vertical modes following Gill (1982). The vertical profile of Brunt–Väisälä frequency and the first three baroclinic modes at 10°S, 60°E are shown in Fig. 9. The first baroclinic mode reaches maximum at the surface and has a zero crossing at around 100 m, which is the position of the thermocline in our model, while the second baroclinic mode reaches a maximum at around 100 m.

The projections of the intraseasonal zonal currents onto the first two modes are shown in Fig. 10. The motions in the first mode are strong in the layers above the thermocline (around 100 m). Generally, they are larger than the motions in other modes. Only during boreal winter and spring are the motions in the second mode comparable to the first mode. In most areas in SWIO, the first mode explains more than 50% of the intraseasonal variability while the second mode explains about 40% of the total variability. However, it turns out that the currents of the second baroclinic mode are mainly responsible for the enhancement of the velocity shear around the thermocline (i.e., for the genesis of OISOs in the SWIO as shown below).

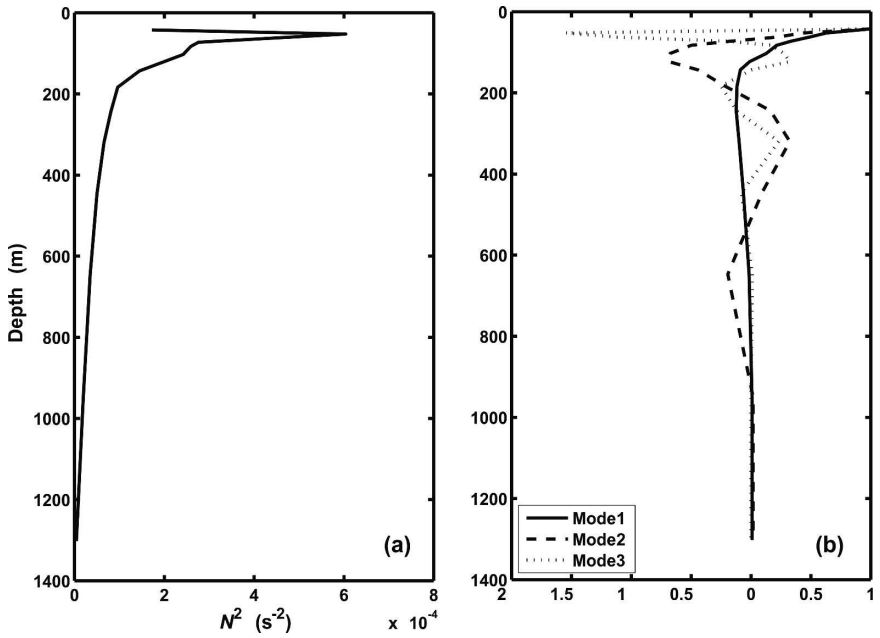

FIG. 9. Vertical profiles of (a) the squared Brunt–Väisälä frequency and (b) the eigenfunctions of the first three baroclinic modes.

The baroclinic energy conversion caused by various baroclinic modes is calculated. If the 20-yr average is taken, the baroclinic conversion of the first mode dominates (Fig. 11). However, as shown above, the OISOs in SWIO are strong in boreal winter and spring. If the average in December is examined, one would find that the second baroclinic mode is the dominant cause for the OISOs, because the baroclinic energy conversion

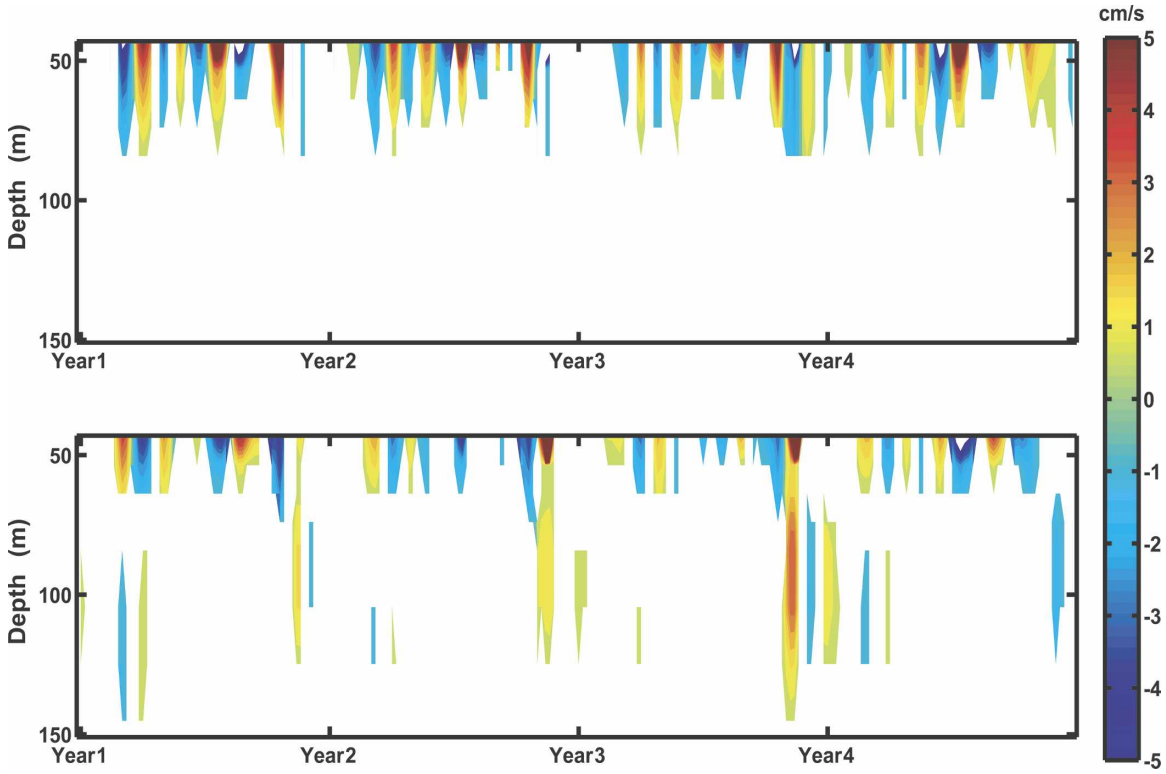

FIG. 10. Projections of intraseasonal velocities onto the first two baroclinic modes in four years.

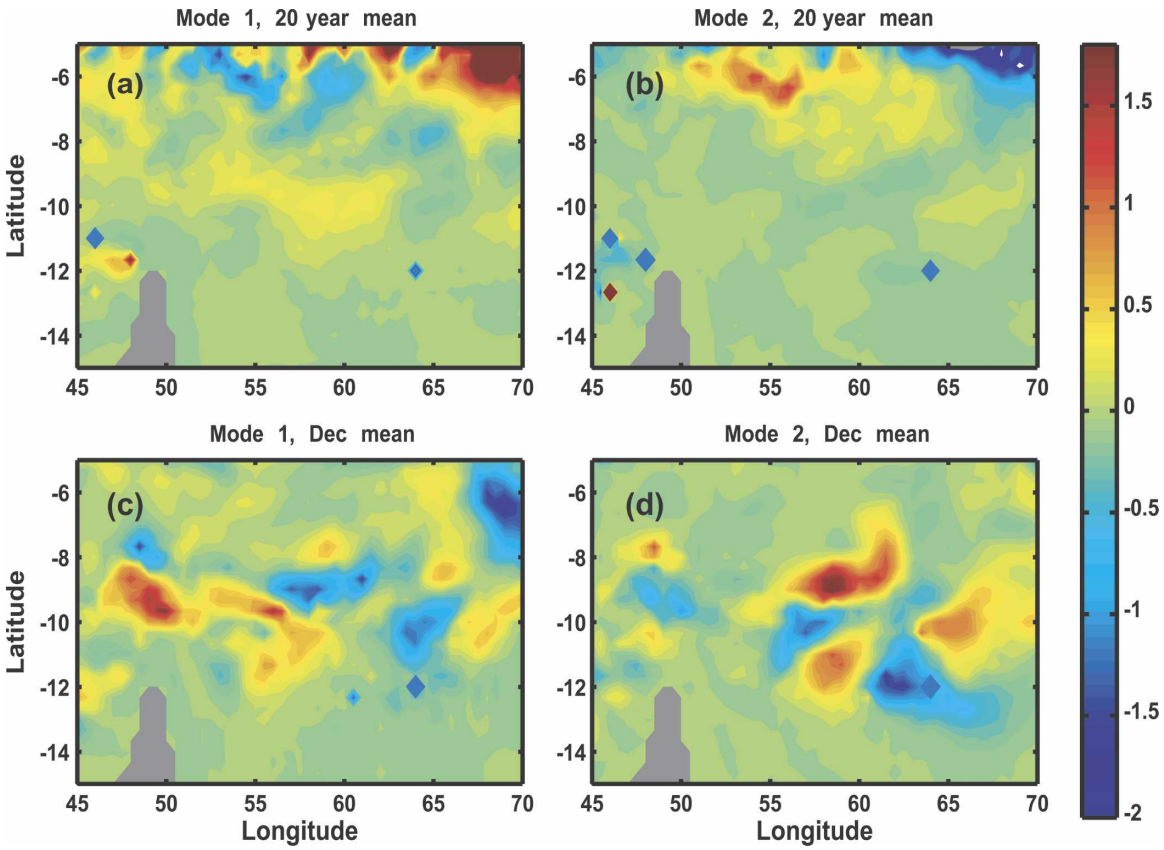

FIG. 11. Baroclinic energy conversion (10^3 W m^{-3}) of the (a) first baroclinic mode, (b) second baroclinic mode, (c) first baroclinic mode in December, and (d) second baroclinic mode in December.

caused by the second mode is slightly larger than that of the first mode (Fig. 11). Therefore, the intensification of baroclinic energy conversion around the thermocline (Fig. 7) is caused by the second baroclinic mode currents (Fig. 10).

Furthermore, enhancement of the currents of the second baroclinic mode indicates the relation between the OISOs in the SWIO and the SEIO. Iskandar et al. (2006) found that the OISOs forced by winds over SEIO off Sumatra were mainly captured by the second baroclinic mode. These wind-driven OISOs propagate westward as baroclinic Rossby waves (Masumoto and Meyers 1998; Xie et al. 2002), leading to baroclinic instability in the SWIO. Thus, the reinforcement of OISOs in SWIO should be significantly influenced, or even determined, by the OISOs in the SEIO. The in-depth analyses of these remote forcings are part of our future study but beyond the scope of this paper.

5. Conclusions and discussion

The OISOs in the SWIO are studied by analyzing a model simulation to demonstrate that they have a period of 40–80 days and propagate westward as Rossby waves, with a phase speed of about 25 cm s^{-1} in boreal winter and spring and have a wavelength of nearly 650 km. The main dynamic reason for OISOs in our model is the baroclinic instability caused by the vertical shear and the density gradients. They are strong in boreal winter and spring, because of the second baroclinic mode waves propagating from the SEIO. Our study indicats that the OISOs in the SWIO have a close relation with those in SEIO.

According to our model, the baroclinic instability is confirmed to be important for OISOs in the SWIO even though we cannot completely exclude the effect of AISOs (A denotes atmospheric) on the OISOs. The first reason is that in the wavenumber spectrum, the high-frequency part of the NCEP reanalysis data decreases much faster than the satellite observations. Thus, the NCEP wind data may not be able to resolve the wind fields with horizontal scale smaller than 800–1000 km (Milliff et al. 2004). Second, parts of the AISOs are excluded in the climatological winds, even though we use weekly mean winds. Therefore, by comparing the model results driven by the interannual wind

stresses and the present model results, the effects of the external forcing and the internal instabilities on OISOs in the SWIO are assumed to be separable for evaluation, which will be reported elsewhere.

The OISOs are an important part of the ocean dynamics in the oceanic mixed layer. In the SWIO, ocean dynamic processes contribute more to the SST variability than the surface heat fluxes do (Klein et al. 1999; Chambers et al. 1999; Murtugudde and Busalacchi 1999). Jochum and Murtugudde (2005) argued that the internal variability with a period of ~100 days is important and may be critical for predicting SSTs in the Indian Ocean, because it may significantly affect the Indian monsoon. Xie et al. (2002) pointed out that the SST variability in SWIO is not locally forced but due to the Rossby waves that propagate from SEIO. Since OISOs in SWIO are enhanced by the second baroclinic mode waves propagating from the SEIO, they are potentially critical to the SST variability. Via their putative impacts on SST, the OISOs probably also have great influence on the rainfall over eastern Africa and have feedbacks to the atmospheric intraseasonal oscillations, like the Madden–Julian oscillations (Waliser et al. 1999), adding to the growing evidence for the importance of this region to regional climate variability. Therefore, OISOs in SWIO need to be better understood. The thermodynamic properties of the OISOs and their feedbacks to the atmosphere are a focus of our future explorations.

Acknowledgments. This work was supported by NASA Indian Ocean Mesoscale Funding and NOAA Coupled Mesoscale Funding. We greatly appreciate the assistance of James Beauchamp and Eric Hackert for preparations of the model data, as well as Dudley Chelton and Ernesto Munoz for helpful suggestions. We also thank two anonymous reviewers for their comments and suggestions.

REFERENCES

Chambers, D. P., B. D. Tapley, and R. H. Stewart, 1999: Anomalous warming in the Indian Ocean coincident with El Niño. *J. Geophys. Res.,* **104,** 3035–3047.

Chen, D., L. M. Rothstein, and A. J. Busalacchi, 1994: A hybrid vertical mixing scheme and its application to tropical ocean models. *J. Phys. Oceanogr.,* **24,** 2156–2179.

Farrar, J. T., and R. A. Weller, 2006: Intraseasonal variability near 10°N in the eastern tropical Pacific Ocean. *J. Geophys. Res.,* **111,** C05015, doi:10.1029/2005JC002989.

Feng, M., and S. Wijffels, 2002: Intraseasonal variability in the South Equatorial Current of the east Indian Ocean. *J. Phys. Oceanogr.,* **32,** 265–277.

Gill, A. E., 1982: *Atmosphere–Ocean Dynamics*. Academic Press, 662 pp.

Han, W., 2005: Origins and dynamics of the 90-day and 30–60-day variations in the equatorial Indian Ocean. *J. Phys. Oceanogr.,* **35,** 708–728.

Iskandar, I., W. Mardiansyah, Y. Masumoto, and T. Yamagata, 2005: Intraseasonal Kelvin waves along the southern coast of Sumatra and Java. *J. Geophys. Res.,* **110,** C04013, doi:10.1029/2004JC002508.

——, T. Tozuka, H. Sasaki, Y. Masumoto, and T. Yamagata, 2006: Intraseasonal variations of surface and subsurface currents off Java as simulated in a high-resolution ocean general circulation model. *J. Geophys. Res.,* **111,** C12015, doi:10.1029/2006JC003486.

Jochum, M., and P. Malanotte-Rizzoli, 2003: On the generation of North Brazil Current rings. *J. Mar. Res.,* **61,** 147–173.

——, and R. Murtugudde, 2005: Internal variability of Indian Ocean SST. *J. Climate,* **18,** 3726–3738.

Kessler, W. S., M. J. McPhaden, and K. M. Weickmann, 1995: Forcing of intraseasonal Kelvin waves in the equatorial Pacific. *J. Geophys. Res.,* **100,** 10 613–10 631.

Klein, S. A., B. J. Soden, and N.-C. Lau, 1999: Remote sea surface temperature variations during ENSO: Evidence for a tropical atmospheric bridge. *J. Climate,* **12,** 917–932.

Masumoto, Y., and G. Meyers, 1998: Forced Rossby waves in the southern tropical Indian Ocean. *J. Geophys. Res.,* **103,** 27 589–27 602.

Milliff, R. E., J. Morzel, D. B. Chelton, and M. H. Freilich, 2004: Wind stress curl and wind stress divergence biases from rain effects on QSCAT surface wind retrievals. *J. Atmos. Oceanic Technol.,* **21,** 1216–1231.

Murtugudde, R., and A. J. Busalacchi, 1999: Interannual variability of the dynamics and thermodynamics of the Indian Ocean. *J. Climate,* **12,** 2300–2326.

——, R. Seager, and A. Busalacchi, 1996: Simulation of tropical oceans with an ocean GCM coupled to an atmospheric mixed layer model. *J. Climate,* **9,** 1795–1815.

——, A. J. Busalacchi, and J. Beauchamp, 1998: Seasonal-to-interannual effects of the Indonesian Throughflow on the tropical Indo-Pacific basin. *J. Geophys. Res.,* **103,** 21 425–21 442.

——, J. P. McCreary Jr., and A. J. Busalacchi, 2000: Oceanic processes associated with anomalous events in the Indian Ocean with relevance to 1997–1998. *J. Geophys. Res.,* **105,** 3295–3306.

Pedlosky, J., 1987: *Geophysical Fluid Dynamics*. 2nd ed. Springer-Verlag, 710 pp.

Potemra, J. T., S. L. Hautala, J. Sprintall, and W. Pandoe, 2002: Interaction between the Indonesian seas and the Indian Ocean in observations and numerical models. *J. Phys. Oceanogr.,* **32,** 1838–1854.

Reppin, J., F. A. Schott, and J. Fischer, 1999: Equatorial currents and transports in the upper central Indian Ocean: Annual cycle and interannual variability. *J. Geophys. Res.,* **104,** 15 495–15 514.

Schott, F., M. Dengler, and R. Schoenefeldt, 2002: The shallow overturning circulation of the Indian Ocean. *Prog. Oceanogr.,* **53,** 57–103.

Sengupta, D., R. Senan, and B. N. Goswami, 2001: Origin of intraseasonal variability of circulation in the tropical central Indian Ocean. *Geophys. Res. Lett.,* **28,** 1267–1270.

Sprintall, J., A. L. Gordon, R. Murtugudde, and R. D. Susanto, 2000: A semiannual Indian Ocean forced Kelvin wave ob-

served in the Indonesian seas in May 1997. *J. Geophys. Res.,* **105,** 17 217–17 230.

Waliser, D. E., K. M. Lau, and J. H. Kim, 1999: The influence of coupled sea surface temperatures on the Madden–Julian oscillation: A model perturbation experiment. *J. Atmos. Sci.,* **56,** 333–358.

——, R. Murtugudde, and L. Lucas, 2003: Indo-Pacific Ocean response to atmospheric intraseasonal variability. Part I: Austral summer and the Madden–Julian oscillation. *J. Geophys. Res.,* **108,** 3160, doi:10.1029/2002JC001620.

Wang, L., C. J. Coblinsky, and S. Howden, 2001: Annual Rossby wave in the southern Indian Ocean: Why does it ''appear'' to break down in the middle ocean? *J. Phys. Oceanogr.,* **31,** 54–74.

Weisberg, R. H., and T. J. Weingartner, 1988: Instability waves in the equatorial Atlantic Ocean. *J. Phys. Oceanogr.,* **18,** 1641–1657.

Xie, S.-P., H. Annamalai, F. A. Schott, and J. P. McCreary Jr., 2002: Structure and mechanisms of south Indian Ocean climate variability. *J. Climate,* **15,** 864–878.

Yu, Z., and J. Potemra, 2006: Generation mechanism for the intraseasonal variability in the Indo-Australian basin. *J. Geophys. Res.,* **111,** C01013, doi:10.1029/2005JC003023.